



Ground-state properties and lattice-vibration effects of disordered Fe-Ni systems for phase stability predictions

Kangming Li  and Chu-Chun Fu 

DEN-Service de Recherches de Métallurgie Physique, CEA, Université Paris-Saclay, F-91191 Gif-sur-Yvette, France

 (Received 23 September 2019; revised manuscript received 11 December 2019; accepted 31 January 2020; published 25 February 2020)

By means of density functional theory, we perform a focused study of both body-centered-cubic (bcc) and face-centered-cubic (fcc) Fe-Ni random solid solutions, represented by special quasirandom structures. The whole concentration range and various magnetic configurations are considered. Excellent agreement on the concentration dependence of magnetization is found between our results and experimental data, except in the Invar region. Some locally antiferromagnetic fcc structures are proposed to approach experimental values of magnetization. Vibrational entropies of ordered and disordered systems are calculated for various concentrations, showing an overall good agreement with available experimental data. The vibrational entropy systematically contributes to stabilize disordered rather than ordered structures and is not negligible compared to the configurational entropy. Free energy of mixing is estimated by including the vibrational and ideal configurational entropies. From them, low- and intermediate-temperature Fe-Ni phase diagrams are constructed, showing a better agreement with experimental data than the one from a recent thermodynamic assessment for some phase boundaries below 700 K. The determined order-disorder transition temperatures for the $L1_0$ and $L1_2$ phases are in good agreement with the experimental values, suggesting an important contribution of vibrational entropy.

DOI: [10.1103/PhysRevMaterials.4.023606](https://doi.org/10.1103/PhysRevMaterials.4.023606)

I. INTRODUCTION

The Fe-Ni alloys are some of the most studied binary systems thanks to their technological interest. They exhibit diverse magnetic and mechanical properties depending on chemical compositions. For example, alloys containing around 36% Ni, also known as Invar, possess vanishingly low thermal expansion coefficients [1], and are widely used where high dimensional stability with temperature is required [2]. Permalloy, with about 80% Ni content, is notable for its high magnetic permeability [3]. The study of the binary alloys is also the first step towards the understanding of multicomponent systems such as austenitic steels and other ferrous alloys.

The phase stability of the Fe-Ni system has been extensively investigated experimentally and theoretically. A comprehensively assessed Fe-Ni phase diagram was constructed by Swartzendruber *et al.* (see Fig. 1 in Ref. [4]). According to the experimental data summarized in Ref. [4], the well-established equilibrium solid phases are body-centered-cubic (bcc) and face-centered-cubic (fcc) random solid solutions, as well as the ordered structure $L1_2$ -FeNi₃ with a critical ordering temperature, noted hereafter as $T_c^{L1_2-\gamma}$, of about 790 K [5].

Less clear is the phase diagram below 600 K, where the diffusion is extremely sluggish and thermodynamic equilibrium cannot be achieved under laboratory conditions. An intermetallic compound $L1_0$ -FeNi was found in meteorites

but disputed to be stable [6] or metastable [7], with a critical ordering temperature, noted hereafter as $T_c^{L1_0-\gamma}$, of 593 K determined from irradiated samples [8]. A yet more controversial issue is the existence of the metastable ordered phase of Fe₃Ni, which was suggested to have a $L1_2$ structure but could not be fully confirmed by experiments [9–11].

On the theoretical side, previous *ab initio* studies were performed for various ordered structures to explore the ground-state properties of Fe-Ni alloys. According to these calculations [12–14], $L1_0$ -FeNi is also a thermodynamically stable phase in addition to $L1_2$ -FeNi₃, while the $L1_2$ -Fe₃Ni has a positive mixing enthalpy. It was also shown that $Z1$ -Fe₃Ni has a lower (but still positive) mixing enthalpy than $L1_2$ -Fe₃Ni [13,14].

However, a systematic first-principles study in bcc and fcc disordered structures is lacking while this is important for the following reasons. First, the energy difference between ordered and disordered phases is crucial for determining the low-temperature phase stability and the order-disorder transition temperatures. Second, although the thermodynamic properties of disordered structures were extrapolated from the *ab initio* data on ordered structures via various methodologies, such as calculation of phase diagrams (CALPHAD) [15], cluster variation method (CVM) [16,17], the embedded atom model (EAM) [18], and magnetic cluster expansion (MCE) [19], the accuracy of such extrapolations need to be verified. Finally, it is known that bcc Fe-Ni alloys are ferromagnetic (FM) on the Fe-rich side, while fcc phases tend to have antiferromagnetic (AF) orderings on the Fe-rich side and FM orderings on the Ni-rich side, but the relative stability between these phases as a function of Ni concentrations is still unclear.

*chuchun.fu@cea.fr

At finite temperatures the vibrational contribution to free energy of Fe-Ni alloys is still an open issue. The vibrational entropy, previously assumed to be negligible [19], was highlighted in the EAM potential study to explain the discrepancy between the calculated and experimental $T_c^{L_{10}\gamma}$ and $T_c^{L_{12}\gamma}$ [18]. Also, the inclusion of the vibrational effects reduces $T_c^{L_{10}\gamma}$ by 40 K in the CVM study [17] and by 480 K in a density functional theory (DFT) study [20]. Consequently, the quantitative effects remain unclear, and previous studies only focused on a very limited concentration range.

Therefore, phase stability of Fe-Ni alloys at low and intermediate temperatures is not fully elucidated due to insufficient experimental information, and on the theoretical side, the lack of an accurate and systematic description of disordered phases at an *ab initio* level. Furthermore, a systematic prediction of vibrational effects on phase stability remains an open issue.

This work is a first-principles study of ground-state properties and lattice vibration effects of disordered Fe-Ni phases for the phase stability prediction at low and intermediate temperatures. We address bcc and fcc disordered configurations, represented by the special quasirandom structures [21], with various magnetic orderings over a broad concentration range, in order to have a systematic understanding of their ground-state magnetic and energetic properties. We perform a detailed analysis on the magnetic configurations around the Invar concentrations to allow a closer comparison with experimental data. We calculate the vibrational entropies of ordered and disordered phases within DFT and discuss its role on the order-disorder transitions by considering available experimental and theoretical results. Free energies of mixing, including vibrational and configurational contributions, and the resulting phase diagrams are obtained from the DFT calculations. These results are compared with a recent CALPHAD study by Cacciamani *et al.* [15] in light of available experimental data.

The paper is organized as follows: The computational details of DFT calculations are introduced in Sec. II. The ground-state energetic and magnetic properties are discussed in Sec. III. In Sec. IV, we present vibrational entropy and free energy of mixing calculated from DFT and compare our results with those from CALPHAD and experiments. Finally, conclusions are presented in Sec. V.

II. COMPUTATIONAL DETAILS

A. Density functional theory method

First-principles calculations were performed using DFT with the projector augmented wave (PAW) method [22,23] as implemented in the Vienna Ab-initio Simulation Package (VASP) code [24–26]. The generalized gradient approximation (GGA) for the exchange-correlation functional in the Perdew-Burke-Ernzerhof parametrization [27] was employed in all the DFT calculations, except in some cases (see Sec. III C), where some local density approximation (LDA) calculations were performed to explore the effect of exchange-correlation functionals. All the calculations are spin polarized. The $3d$ and $4s$ electrons were considered as valence electrons. The plane-wave basis cutoff was set to 400 eV. The Methfessel-Paxton broadening scheme with a smearing

width of 0.1 eV was used [28]. The convergence cut-off for the electronic self-consistency loop was set to $\Delta E = 10^{-6}$ eV. The k -point grids used in our calculations were adjusted according to the cell size to achieve a k -sampling equivalent to a cubic unit cell with a $16 \times 16 \times 16$ shifted grid following the Monkhorst-Pack scheme [29]. Atomic magnetic moments were obtained by an integration of spin-up and spin-down charge densities within the PAW spheres, with a radius of 1.302 Å (respectively, 1.286 Å) for Fe (respectively, Ni).

Disordered alloys were represented by special quasirandom structures (SQSs) [21] with minimized Warren-Cowley short-range order parameters [30,31]. The ground-state properties of bcc and fcc FM disordered structures were calculated using $4 \times 4 \times 4$ 128-atom and $3 \times 3 \times 3$ 108-atom supercells, respectively, while the calculations in fcc antiferromagnetic double layer (AFD) structures were done in $4 \times 4 \times 4$ 128-atom supercells on the body-centered tetragonal lattice with an initial c/a ratio equal to $\sqrt{2}$. The structures were initialized with the desired magnetic ordering. Magnetic structure, atomic position, cell shape, and volume were fully relaxed to ensure a maximum residual force of 0.02 eV/Å and a maximum residual stress of 3 kbar.

Vibrational entropy S_{vib} was obtained within the harmonic approximation from the frozen phonon calculations in $3 \times 3 \times 3$ supercells using VASP and PHONOPY [32]. Before performing the frozen phonon calculations, supercells were first fully relaxed with a maximum residual force of 0.001 eV/Å and a maximum residual stress of 1 kbar. For pure and ordered phases, the difference in S_{vib} between $3 \times 3 \times 3$ and $2 \times 2 \times 2$ supercells is less than 0.02 k_B /atom. We check that the difference in S_{vib} between two different fcc FM SQSs at 50% Ni is less than 0.02 k_B /atom, so the results obtained from one SQS are representative for the disordered structures at a given concentration.

The mixing enthalpy (per atom) of a structure $\text{Fe}_{1-x}\text{Ni}_x$ is defined as follows:

$$\Delta H_{\text{mix}} = H(\text{Fe}_{1-x}\text{Ni}_x) - (1-x)H(\text{Fe}) - xH(\text{Ni}), \quad (1)$$

where x is the Ni concentration, $H(\text{Fe}_{1-x}\text{Ni}_x)$ is the enthalpy (per atom) of the structure, and $H(\text{Fe})$ and $H(\text{Ni})$ are the enthalpy (per atom) of Fe and Ni in the reference states, respectively. The vibrational entropy of mixing (per atom) and the free energy of mixing (per atom) are defined in the similar manner.

Finally, it should be noted that all the alloy concentrations given in the paper are expressed in the atomic percentage of Ni.

B. Validation of the DFT approach

In this section, we validate the present approach by comparing the results of the pure and ordered phases with previous calculations. Detailed information on equilibrium lattice parameters, magnetic moments, and energies is given in the Supplemental Material [33–38].

Various collinear magnetic structures of Fe and Ni have been considered. The obtained ground-state properties agree well with recent calculations [12,14,39] (see Ref. [33] for details). We confirm that the ground state of Fe and Ni is bcc FM and fcc FM, respectively. The collinear magnetic ground state of fcc Fe is the AFD structure, which transforms

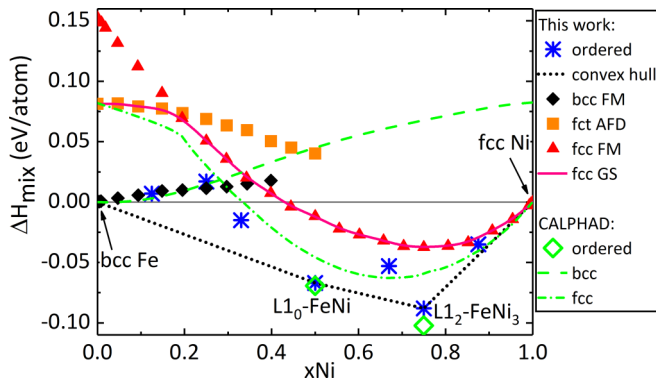


FIG. 1. Mixing enthalpies of ordered and disordered structures. Note that the reference states are bcc FM Fe and fcc FM Ni. The dotted line denotes the convex hull. The solid line denotes the ground-state mixing enthalpies of the fcc random solutions. Results from the CALPHAD assessment by Cacciamani *et al.* are shown for comparison [15].

spontaneously into a face-centered-tetragonal (fct) AFD structure on volume relaxation. Therefore, bcc FM Fe and fcc FM Ni are taken as the reference states, except where the fct AFD phase is taken as the reference state of Fe to allow direct comparison with previous calculations (see Sec. III A).

We performed DFT calculations in the ordered structures presented in Refs. [12,13]. The results of the mixing enthalpies agree well with those by Mishin *et al.* [12] (see Ref. [33] for details). In addition, our results agree with Refs. [13,14] that the most stable phase of Fe₃Ni is the fct Z1 structure, though its mixing enthalpy is still positive. There are five FM structures with a negative mixing enthalpy: the experimentally observed phases L1₂-FeNi₃ and L1₀-FeNi, and cI32-FeNi₇, C11_f-Fe₂Ni, and C11_f-FeNi₂. As demonstrated in the following discussion, only the two experimentally observed phases are thermodynamically stable.

III. GROUND-STATE PROPERTIES

A. Mixing enthalpies

Figure 1 shows the mixing enthalpies of the SQSs and the most stable ordered structures. The bcc SQSs with more than 40% Ni transform into an orthorhombic lattice after relaxation, which is associated with the instability of bcc Fe-Ni alloys at higher Ni concentrations. Therefore, the bcc phases above 40% Ni shall not be considered in the following. As in the case of AFD Fe, fcc AFD SQSs also transform spontaneously into fct AFD structures with the *c/a* ratio decreasing with increasing Ni concentrations.

Overall, the ordered structures have a lower energy than the SQSs. L1₂-FeNi₃ and L1₀-FeNi form the convex hull with bcc Fe and fcc Ni and thus are the only ground states of Fe-Ni alloys. We note that the energy of L1₀-FeNi is just 0.008 eV/atom below the line connecting the energies of bcc Fe and L1₂-FeNi₃. The most stable state of SQSs is FM, with the bcc-fcc crossover at about 37% Ni. As the fct AFD state is more stable than the fcc FM one below 18% Ni, the energy curve of the fcc disordered ground states consists of the AFD and FM branches. The predicted AFD-FM crossover is higher

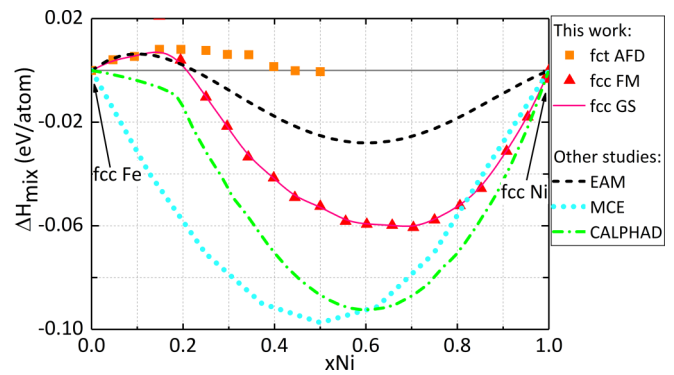


FIG. 2. Comparison of mixing enthalpies of fcc disordered structures between this work and previous calculations (EAM [18], CALPHAD [15], and MCE [19]). The reference state of Fe is the fct AFD phase in this study, and the fcc antiferromagnetic state in other approaches [15,18,19]. The solid line represents the ground-state mixing enthalpies of fcc disordered structures by DFT.

than the value from another DFT-GGA study [40] because the latter did not consider the tetragonal deformation of the AFD phase and may consequently underestimate its stability.

To our best knowledge, there is no existing result of the mixing energies for bcc and fcc Fe-Ni disordered phases from first-principles studies. Recently, Cacciamani *et al.* [15] performed a comprehensive CALPHAD thermodynamic assessment of the Fe-Ni system. The ground-state mixing enthalpies ΔH_{mix} of the random solid solutions and the L1₀-FeNi and L1₂-FeNi₃ phases predicted by this CALPHAD assessment are shown in Fig. 1 for comparison. Both approaches predict similar ΔH_{mix} for the bcc random solid solutions below 40% Ni and the ordered structures. But the energies of fcc random solid solutions predicted from CALPHAD are systematically lower than from DFT, especially in the concentrated concentration range.

Comparison of ΔH_{mix} of the fcc random solid solutions can also be made with the recent EAM [18] and MCE [19] studies, as shown in Fig. 2. Our energy curve is between those from the EAM potential study [18] and the CALPHAD calculations [15] with a similar shape, namely concave below 20% Ni and convex above, indicating a change of magnetic order. The energy curve from the MCE study [19] is rather symmetric with respect to the concentration and does not seem to reflect the change of magnetic order near pure Fe. We note that no *ab initio* data of random alloys were used during the fitting procedure in these previous studies [15,18,19]. The discrepancy between the present study and the previous calculations thus suggests the need for an improved prediction by considering reliable first-principles results in random solid solutions.

Being much higher in energy than the most stable FM SQSs, the fct AFD phase is only metastable and not relevant to the stable phase equilibrium. Therefore, the AFD phase is not discussed in the following sections.

B. Magnetic properties

The calculated magnetization of the most stable SQSs were compared to the available experimental data [41,42] in Fig. 3(a). Experimentally, the magnetization at 0 K is

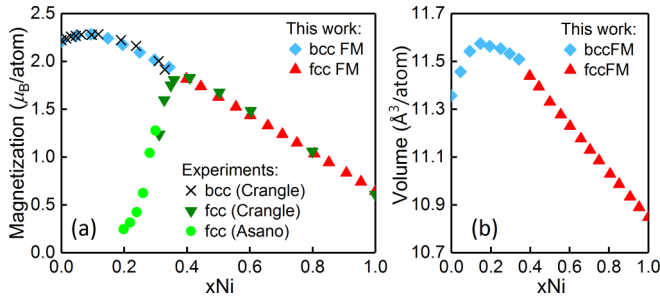


FIG. 3. (a) Magnetization and (b) average volume of the most stable disordered structures. Experimental magnetization data by Crangle and Hallam [41] and Asano [42].

extrapolated from a series of measurements on the spontaneous magnetization at various temperatures. The experimental magnetization of bcc (respectively, fcc) alloys below (respectively, above) the bcc-fcc crossover is well reproduced by our calculations. For the fcc alloys below the crossover, since the magnetic order changes gradually from FM to AF with decreasing Ni concentrations, the magnetic structures in this concentration region cannot be well described by the FM or AFD structures but will be further discussed in Sec. III C.

The variation in the magnetization is correlated with the variation in the atomic volume. As shown in Fig. 3(b), the average volume changes nonlinearly with Ni concentrations in the bcc FM SQSs but varies linearly in the fcc FM SQSs at a rate similar to the experimental value [43].

For the fcc FM SQSs, as the concentration dependence of Fe and Ni moments is not significant [33], the magnetic dilution effect is dominant and results in an almost linear decrease in the magnetization with Ni concentrations. For bcc FM SQSs, however, the magnetization first increases due to the strong increase in Fe moments with Ni concentrations ($0.23 \mu_B$ per 10% Ni [33]). Then the magnetization decreases again because Fe moments increase at a slower rate ($0.06 \mu_B$ per 10% Ni [33]) and the magnetic dilution effect becomes dominant again. Please note that the Fe and Ni moments do not necessarily follow the trend of the magnetization and have local-composition dependence [44]. Indeed, it is found that the local chemical environment has a large impact on the magnetic moments than the local atomic volumes [33].

C. Discussion on magnetization in the Invar region

In the relatively dilute fcc Fe-Ni alloys below 36% Ni, due to the change of the magnetic ordering tendency between the AFD (low-Ni) and the FM (high-Ni) configurations, some intermediate magnetic structures are expected, in particular the locally antiferromagnetic (LAF) structures as suggested in Refs. [45,46] where the spin of Fe with few Ni neighbors is antiparallel to the global magnetization. Other noncollinear configurations were also proposed [47]. Here we propose some LAF structures with 25 to 35% Ni (see Ref. [33] for details) in order to approach the experimental magnetization values. The magnetization of the LAF structures is shown in Fig. 4 with those of fcc FM structures and from experiments. For the LAF structures, magnetization decreases with increasing number of the AF Fe sites. The experimental magnetization is covered in the range of the calculated values.

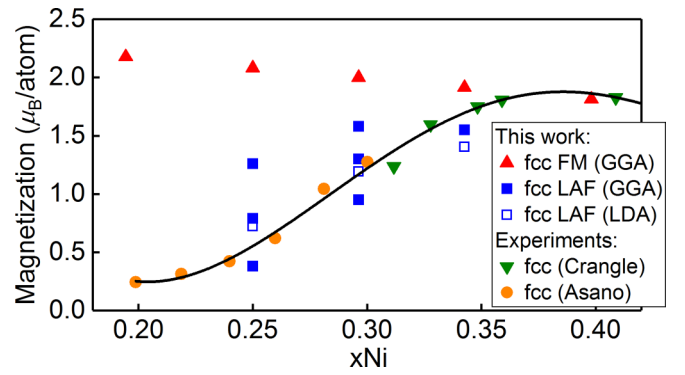


FIG. 4. Magnetization of the fcc FM and LAF structures in the Invar region from the present DFT study compared to experimental data by Crangle and Hallam [41] and Asano [42]. The black line guides for the experimental trend. The magnetization of the LAF structures calculated from LDA is also shown for comparison, being slightly below the value calculated from GGA. Only one LAF structure for each concentration is recalculated using LDA.

In these calculations, the energy of a structure increases with the number of the AF Fe sites. The LAF state is only metastable and has a higher energy than the FM state in the fcc Fe-Ni alloys with down to 25% Ni. This is consistent with Refs. [40,46] but at variance with previous LDA calculations [45–47]. Indeed, Ruban *et al.* [46] showed that the fcc magnetic ground state at 35% Ni at the experimental a_0 is LAF in LDA but purely FM in GGA. This is confirmed in our calculations using LDA in the same FM and LAF structures from 25% to 34% Ni (see Ref. [33] for details). The magnetization of the LAF structures using LDA is slightly smaller than the value in the same structures in the GGA calculations (Fig. 4). However, the LDA results should be treated with caution because LDA fails to predict not only the aforementioned equilibrium a_0 but also the ground state of iron [48,49].

Therefore, the energetic stability of the fcc structures between 25 and 34% Ni is very sensitive to the adopted exchange-correlation functionals. Furthermore, there may be other magnetic structures with similar energies and magnetization but different from the proposed LAF configurations. In particular, the choice of the set of AF Fe sites is not unique. Indeed, it was shown in Ref. [40] that there are a large number of magnetic configurations close in energy in Fe-rich Fe-Ni structures in small volumes, resulting in large magnetic entropy and leading to Invar effects.

IV. FINITE-TEMPERATURE PROPERTIES

The phase stability under constant pressure is governed by the Gibbs free energy of mixing ΔG_{mix} , which is related to the mixing enthalpy ΔH_{mix} and the entropy of mixing ΔS_{mix} as follows:

$$\Delta G_{\text{mix}} = \Delta H_{\text{mix}} - T \Delta S_{\text{mix}}, \quad (2)$$

where ΔH_{mix} and ΔS_{mix} are calculated with respect to bcc Fe and fcc Ni. Approximations are needed to evaluate ΔG_{mix} . In the first place, we assume ΔH_{mix} to be temperature independent, i.e., equal to the ground-state ΔH_{mix} . The entropy term

can have various sources such as the electronic contribution, magnetism, chemical configuration, and lattice vibration. The electronic entropy is usually small [20], while the magnetic entropy is less important in this study since we focus on the temperatures below the magnetic transition. Both the electronic and magnetic contributions are consequently ignored in the present study, but it is noted that they can be addressed, e.g., in bcc Fe by combining various techniques [50].

The configurational entropy is zero for the perfectly ordered structures but is usually considered to be dominant for the random solid solutions. The ideal configurational entropy $\Delta S_{\text{conf}}^{\text{ideal}}$ is often used to approximate the true configurational entropy of disordered alloys and thus will be used in our estimation of ΔG_{mix} . However, we note that the configurational entropy can also be treated using more sophisticated techniques [17].

As highlighted in Ref. [18], lattice vibration is another important contribution to entropy and is considered for FM alloys in this work. Some recent theoretical studies [51–53] investigated the impact of magnetic excitations on lattice excitations in pure Fe and Ni. However, as we focus on chemical phases and their transitions below the Curie points, we neglect such effects in the determination of the vibrational entropies.

In the following, we first present the results of the vibrational entropies (Sec. IV A), which are then used to estimate ΔG_{mix} (Sec. IV B). Based on these DFT results, the phase diagrams are constructed (Sec. IV C) and the vibrational effects on the phase transitions are discussed (Sec. IV D).

A. Vibrational entropy

Due to the high computational cost, we limit the calculated phases to the most relevant ones at finite temperatures, which include the stable phases at very low temperatures, namely bcc FM Fe, fcc FM Ni, $L1_2$ -FeNi₃ and $L1_0$ -FeNi, and bcc FM and fcc FM random solid solutions for some Ni concentrations.

The vibrational entropies of mixing of the studied phases increase with increasing temperatures and saturate above 300 K. The saturated vibrational entropies of mixing at 300 K are shown in Fig. 5. We also show the ideal configurational entropy $\Delta S_{\text{conf}}^{\text{ideal}}$ for comparison, which is often used to approximate the true configurational entropy and has the following form:

$$\Delta S_{\text{conf}}^{\text{ideal}} = -k_B(x_{\text{Fe}} \ln x_{\text{Fe}} + x_{\text{Ni}} \ln x_{\text{Ni}}). \quad (3)$$

For the SQSs, $\Delta S_{\text{vib,mix}}$ is of the same order of magnitude of $\Delta S_{\text{conf}}^{\text{ideal}}$ and thus not negligible. The fcc FM SQSs have a larger $\Delta S_{\text{vib,mix}}$ than the ordered ones, suggesting the chemical ordering reduces the vibrational entropy.

Recently, Lucas *et al.* [54] obtained the partial phonon densities of states (DOS) of Fe and Ni, defined as the contribution from the given species to the total phonon DOS, at 300 K in fcc Fe-Ni samples through inelastic neutron scattering and nuclear resonant inelastic x-ray scattering. The experimentally derived partial and total vibrational entropies are compared to the DFT values in Fig. 6. The overall agreement is reasonably good: The differences between the calculated and measured values for the partial S_{vib} of Fe and Ni and total S_{vib} are less than 0.07, 0.11, and 0.05 k_B/atom , respectively. Both

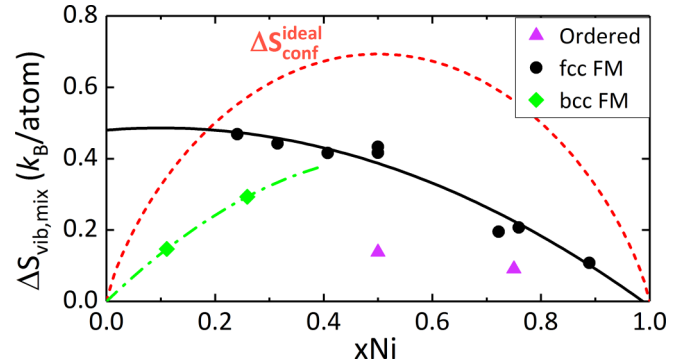


FIG. 5. Vibrational entropies of mixing of ordered and disordered structures as functions of Ni concentrations at 300 K. Note that the reference states are bcc FM Fe and fcc FM Ni. The solid and dash-dotted lines are the second-order polynomial fits of the fcc and bcc DFT data, respectively. The ideal configurational entropy is plotted for comparison.

our work and the experiment [54] confirm that the chemical ordering reduces S_{vib} , but the change in S_{vib} due to the $L1_2$ -disorder transition is smaller in the experiment. Indeed, the ordered sample obtained in the experiment has a small long-range order parameter of 0.37 and does not correspond to a fully equilibrated ordered state at 300 K [54]. The actual S_{vib} of the perfectly $L1_2$ phase can be further reduced and the actual difference between the perfectly $L1_2$ and the disordered phases would be larger than this experimental difference.

B. Free energy of mixing of disordered structures

We evaluate ΔG_{mix} using the following form:

$$\Delta G_{\text{mix}} = \Delta H_{\text{mix}}^{\text{GS}} - T(\Delta S_{\text{conf}}^{\text{ideal}} + \Delta S_{\text{vib,mix}}). \quad (4)$$

Here $\Delta H_{\text{mix}}^{\text{GS}}$ is the ground-state mixing enthalpy obtained in Sec. III A. $\Delta S_{\text{conf}}^{\text{ideal}}$ is the ideal configurational entropy calculated from Eq. (3) for bcc and fcc FM SQSs and zero for ordered structures. $\Delta S_{\text{vib,mix}}$ is the vibrational entropy of mixing obtained in Sec. IV A.

Thermodynamic data from experiments in Fe-Ni alloys were obtained at temperatures generally higher than 1000 K [15], while such data at lower temperatures are often assessed through empirical approaches such as CALPHAD. In a recent CALPHAD modeling of the Fe-Ni system by Cacciamani *et al.* [15], the mixing enthalpies and the activity coefficients of the fcc PM phase fit well with high-temperature experimental results. However, the CALPHAD prediction is not ensured to be accurate for the low-temperature bcc and fcc FM phases and should be further validated with other methodologies.

Figure 7 shows a comparison between our DFT results and the CALPHAD prediction for the free energies of mixing of bcc and fcc FM solid solutions. For the bcc phase, both methods predict similar $\Delta G_{\text{mix}}^{\text{bcc}}$ below 6% Ni, the maximum solubility of Ni in bcc solid solutions [15], but the degree of agreement above 6% Ni decreases with increasing temperatures. As the CALPHAD model was fitted mostly on the thermodynamic data of the fcc phase, its description of the bcc phase is expected to be less accurate and needs to be revisited. For the fcc phase, the results are compared down

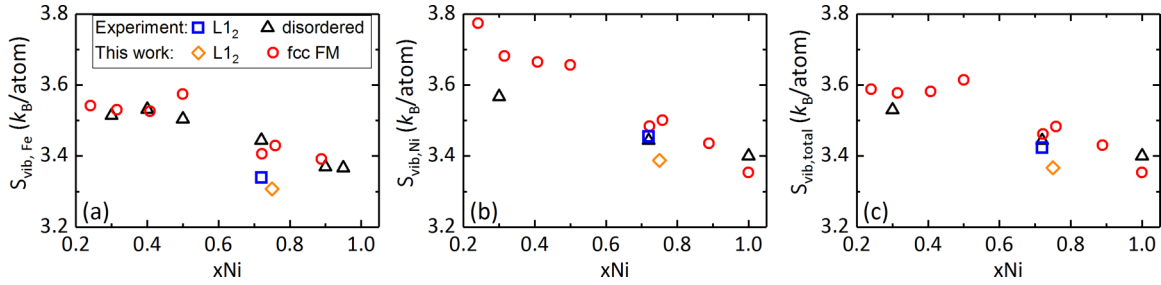


FIG. 6. Partial vibrational entropies of (a) Fe and (b) Ni and (c) total vibrational entropies of fcc FM SQSs at 300 K from the present DFT study compared to the experimental data of fcc ordered and disordered samples at the same temperature [54].

to the bcc-fcc crossover predicted by DFT near 35% Ni. The best agreement between CALPHAD and DFT is observed at 500 K, while the energies predicted by DFT and CALPHAD differ by at most 0.015 eV/atom at 300 and 700 K. The reason why the best agreement in $\Delta G_{\text{mix}}^{\text{fcc}}$ is achieved at 500 K may be understood as follows. Since the CALPHAD assessment mainly utilized experimental data above 1000 K, its prediction is more reliable at high temperatures, while our DFT results are more reliable at low temperatures. Therefore, the CALPHAD results may be more reliable at 700 K where the magnetic disordering effect neglected in this work becomes non-negligible. However, our approximations are well grounded at lower temperatures, while the extrapolation of CALPHAD from high temperatures above 1000 K is more questionable. Therefore, we believe our DFT calculations give more accurate results at 300 K. In the intermediate temperature range the two approaches are both valid and agree with each other, which may be seen rather as a cross-validation between the two methods.

C. Phase diagrams

In this section, we compare the DFT-predicted phase diagrams with the CALPHAD ones by Cacciamani *et al.* [15] and experimental data. Experimentally, it is not completely clear whether $L1_0$ -FeNi is stable [6] or metastable [7], while the present and the previous first-principles calculations [12–14,16] support the former. Consequently, we first compare the theoretical and experimental phase diagrams including only the experimentally well-established phases, namely without $L1_0$ -FeNi. Then we propose a phase diagram including all the theoretically predicted stable phases (including the $L1_0$ -FeNi phase) and discuss it in the light of

the available experimental data, including the order-disorder transition temperature of $L1_0$ -FeNi determined in irradiated alloys. By comparing the two phase diagrams, we can also gain insights into how $L1_0$ -FeNi affects the phase diagram.

The following notations are used for the convenience of discussion. The bcc random solid solution with low Ni content, FM below 1000 K, is termed α ; γ represents the fcc random solid solution, with γ_{PM} and γ_{FM} specifying the magnetic order; $L1_2$ (respectively, $L1_0$) denotes the stoichiometric and off-stoichiometric $L1_2$ -FeNi₃ (respectively, $L1_0$ -FeNi) ordered phase. The phase boundary separating a two-phase region $A + B$ and a single-phase region B is noted as $A + B/B$.

In this work, the widely used common tangent construction of phase diagram (see, e.g., Refs. [19,55]) is applied, using the free energies of mixing of the considered phases. At each temperature, the equilibrium concentrations of the two phases are determined from the points of contact between the free-energy-versus-concentration curves of the two phases and their common tangent. We use the free energies of mixing of the SQSs for the random solid solutions as they are known to be representative for disordered alloys [40,56–61]. For the stoichiometric $L1_2$ and $L1_0$ phases, we use the perfectly ordered structures as in many other theoretical studies (see, e.g., Refs. [19,62,63]).

For the off-stoichiometric $L1_0$ and $L1_2$ phases (in the range of 40–60% and 60–90% Ni, respectively), we consider the presence of antisites as in the CALPHAD and CVM approaches [15,17,64,65] to account for the deviation from the stoichiometric ordered structures. For the $L1_2$ and $L1_0$ phases below (respectively, above) the stoichiometric Ni concentrations, we assume that the Fe (respectively, Ni) sublattice is fully occupied by the Fe (respectively, Ni) atoms, while

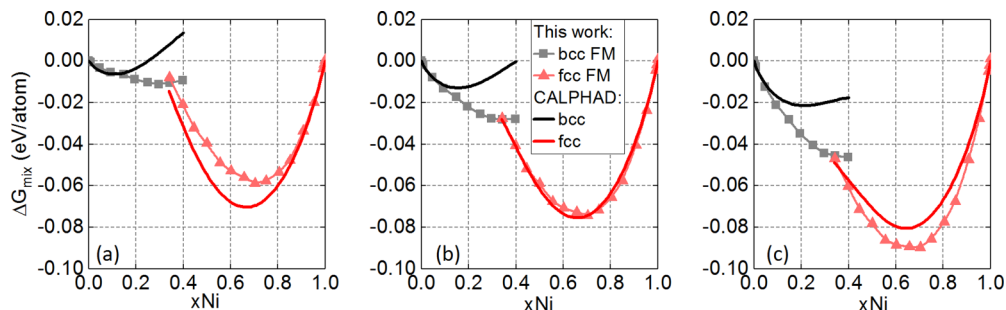


FIG. 7. Comparison of ΔG_{mix} of random solid solutions at (a) 300 K, (b) 500 K, and (c) 700 K between this study and the CALPHAD assessment by Cacciamani *et al.* [15]. Note that the reference states are bcc Fe and fcc Ni.

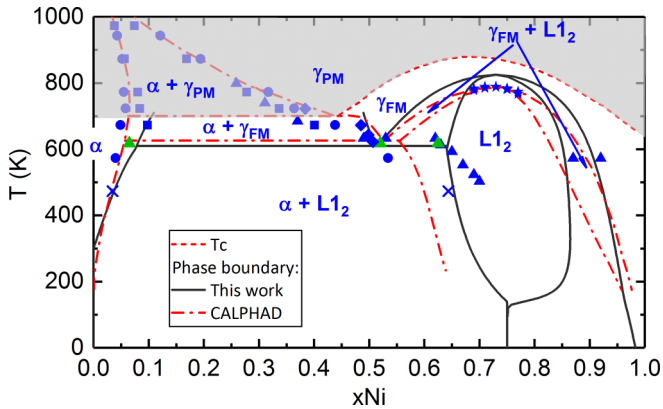


FIG. 8. Comparison of the phase diagrams (without $L1_0$) from the present DFT study, the CALPHAD prediction by Cacciamani *et al.* [15] and the experiments. Experiments: Circle [66], triangle [67], star [5], cross [7], square [68], and diamond [69]. The shaded zone is the phase regions involving the equilibrium with γ_{PM} . The triangles in green mark the eutectoid equilibrium. The T_{Curie} curve is from the CALPHAD prediction [15], which agrees well with experimental data summarized in Ref. [70].

the additional Fe (respectively, Ni) atoms are distributed as antisites on the Ni (respectively, Fe) sublattice. However, even with this assumption there are still a large number of possible distributions of the antisites. For simplicity, we considered two types of the antisite distributions: (1) The antisites are randomly distributed and (2) the pairs consisting of two first-nearest-neighbor antisites are randomly distributed (see Ref. [33] for details). Such arrangements of atoms allow a strong long-range order (LRO) and a short-range order (SRO) close to that of the stoichiometric ordered structures. For example, for the generated off-stoichiometric $L1_0$ structure with 60% Ni, its SRO parameters for the first two shells and the LRO parameter are respectively $[-0.25, 0.72]$ and 0.8, compared with $[-0.33, 1.00]$ and 1 for the stoichiometric $L1_0$ -FeNi, and $[0.00, 0.00]$ and 0 for the SQS at the same concentration. Also, the first type of configuration is chosen since we are particularly interested in a good description around the order-disorder transitions, and it exhibits the highest configurational entropy within the current assumption. And the second type is considered as they have a lower energy for certain concentrations while still having a large configurational entropy. The free energies of mixing of these two types of off-stoichiometric ordered structures were calculated from DFT. Then the configurations with a lower free energy were used to represent the off-stoichiometric phases at a given concentration: The configurations of the first type have a lower free energy for the $L1_0$ phase below 50% Ni, and the $L1_2$ phase below and above 75% Ni, while the configurations of the second type are energetically more favorable for the $L1_0$ phase above 50% Ni.

1. Phase diagram excluding $L1_0$

Figure 8 shows the DFT-predicted phase diagram without the $L1_0$ phase compared to the CALPHAD prediction [15] and the representative experimental data. Comprehensive experimental references can be found in Refs. [4,15].

The phase equilibria between the α and fcc phases (γ and $L1_2$) were investigated using samples cooled under laboratory conditions [66–69] and meteorites [7]. It was concluded in Ref. [67] that γ_{FM} with 52% Ni decomposes eutectoidally into α with 6.5% Ni and $L1_2$ with 62.5% Ni at 618 K (triangles in green), which was widely accepted in the construction of the phase diagrams [4,7,15,71,72]. The study on meteorites [7] concluded that α equilibrates with $L1_2$ at 473 ± 50 K, but the equilibrium Ni concentration of $L1_2$ is lower than those from Ref. [67]. It is also noted that in the study of Ref. [66] no ordered structure was detected even at 573 K. According to the authors of this study [66], the ordered phases $L1_0$ and $L1_2$ may develop at lower temperatures, may not be easily detected by electron diffraction techniques, or may be kinetically restricted in their formation.

The $\gamma_{FM} + L1_2$ equilibrium was examined in a Mössbauer spectroscopy study on samples with 69–77% Ni [5] and in Ref. [67] where the phase boundaries $L1_2/L1_2 + \gamma_{FM}$ and $L1_2 + \gamma_{FM}/\gamma_{FM}$ at 573 K were determined (triangles around 90% Ni in Fig. 8).

It can be seen from Fig. 8 that the major difference between CALPHAD and the experimental results comes from the phase boundaries $\alpha + L1_2/L1_2$, $L1_2/L1_2 + \gamma_{FM}$, and $L1_2 + \gamma_{FM}/\gamma_{FM}$ below 700 K. In particular, the Ni concentration of $L1_2$ of the eutectoid decomposition from CALPHAD is 55.5%, 7% Ni lower than the experimental value.

The DFT-predicted phase diagram is in overall good agreement with the experimental data. The major discrepancy is a calculated maximum of $T_c^{L1_2-\gamma}$ 40 K higher than the measured value of 790 K [5]. We predict the eutectoid reaction occurs at 610 K between α with 7.8% Ni, γ_{FM} with 51.6% Ni, and $L1_2$ with 64% Ni, in good agreement with Ref. [67] (triangles in green). Compared with the CALPHAD prediction below 700 K, our predicted phase boundaries of the $\alpha + L1_2$ and $\gamma_{FM} + L1_2$ two-phase regions agree better with the measurements in Refs. [7,67,69]. We note the boundary $L1_2/L1_2 + \gamma_{FM}$ below 500 K is quite different between DFT and CALPHAD: The former predicts a retrograde solubility of Ni in $L1_2$ with a maximum of 86% Ni, whereas in the latter the solubility of Ni in $L1_2$ tend to increase with decreasing temperatures.

It is worth mentioning that the phase boundaries $\alpha/\alpha + \gamma_{FM}$ and $\alpha + \gamma_{FM}/\gamma_{FM}$ (shaded area in Fig. 8) are absent in the DFT phase diagram as the magnetic disordering effects are not considered in this work. Though magnetic excitations can occur below T_{Curie} , their effects on the phase boundaries between γ_{FM} and $L1_2$ are expected to be minor because experimentally T_{Curie} are around 100 K higher than the order-disorder transition temperatures. Indeed, the magnetic disordering/ordering effects on phase stability can be elucidated by comparing the DFT-predicted and experimental phase diagrams. According to the DFT-predicted phase diagram, without the magnetic disorder the γ_{FM} single-phase region would be smaller and $T_c^{L1_2-\gamma}$ would be higher. The latter is consistent with the finding that an extremely high external magnetic field leads to an increase in $T_c^{L1_2-\gamma}$ [73]. Our results also indicate that without magnetic disorder the solubility of Ni in α increases with increasing temperatures, while the experimental data exhibit a retrograde solubility with a maximum at ~ 700 K, close to T_{Curie} of γ_{FM} at the equilibrium concentration. This

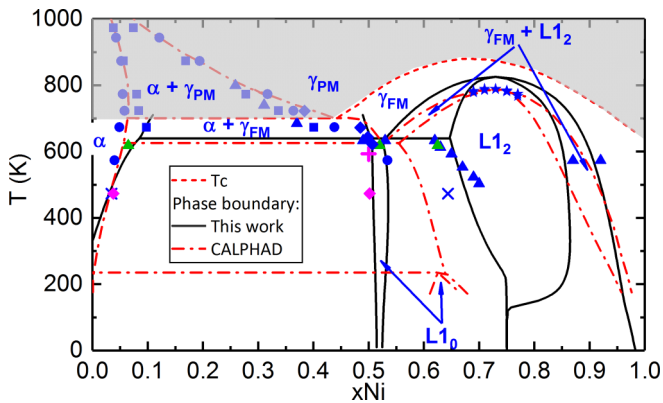


FIG. 9. Comparison of the phase diagrams (with $L1_0$) from the present DFT study, the CALPHAD assessment by Cacciamani *et al.* [15], and the experiments [5–8,66–69,81]. Diamonds are the lower and upper boundaries of the $\alpha + L1_0$ two-phase region from the measurements in meteorites [6]. The plus symbol denotes $T_c^{L1_0-\gamma}$ obtained from the irradiation experiments [8,81]. Other notations are the same as in Fig. 8.

suggests that the experimental retrograde solubility in α is related to the emergence of magnetic disorder in γ_{FM} .

The above effects can be understood as follows: Since magnetic disorder is more significant for the phase with lower T_{Curie} than the one with higher T_{Curie} at the same temperature, the magnetic entropy stabilizes γ_{FM} with respect to both α and $L1_2$ as the experimental T_{Curie} of γ_{FM} is lower than the other two phases [5,74,75].

2. Phase diagram including $L1_0$

The $L1_0$ phase is known to exist in meteorites [6,7,76,77] and can be obtained by annealing with various special techniques to promote atomic diffusion [78–80]. It was concluded as a stable phase by Reuter *et al.* [6], who found only the equilibrium between α and $L1_0$ in meteorites but did not observe $L1_2$. However, another meteorite study found that α equilibrates with $L1_2$ instead of $L1_0$ at 473 ± 50 K [7] and thus concluded the $L1_0$ phase to be metastable. But the equilibrium concentration of $L1_2$ obtained in this study [7] is inconsistent with those found in Ref. [67] (see triangles and crosses in Fig. 9). The lack of a clear conclusion from meteorite studies is due to the lack of true equilibria in meteorites even after more than 10^8 years of slow cooling (<1 atomic jump per 10^4 years at 573 K) [6,7]. It is shown that under irradiation the $L1_0$ ordering occurs in the initially disordered alloys [8,81,82]. It is argued that the obtained $L1_0$ phase is not a metastable phase induced by irradiation effects but rather a stable phase whose formation rate is enhanced by irradiation effects [81,82].

On the theoretical side, the $L1_0$ phase is predicted to be stable in the recent first-principles and phenomenological calculations [12–14,16,83] and is presented in the recent theoretical phase diagrams [15,18,68,84]. Both this study and the CALPHAD assessment by Cacciamani *et al.* [15] suggest the $L1_0$ phase as a stable phase to be included in the phase diagram, as shown in Fig. 9.

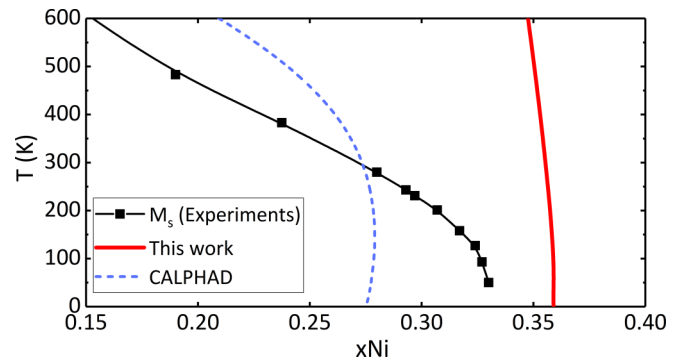


FIG. 10. Comparison of the experimental martensitic start temperature curve M_S [64], and the T_0 curves from our DFT calculations, the CALPHAD assessment by Cacciamani *et al.* [15].

According to our results, $L1_0$ is stable below $T_c^{L1_0-\gamma}$ and equilibrates with α and $L1_2$ on the Fe-rich and Ni-rich sides, respectively. However, as the energy of $L1_0$ -FeNi lies very close to the line connecting the energies of bcc Fe and $L1_2$ -FeNi₃ (Fig. 1), its stability can be very sensitive to external perturbations (impurity in meteorites, irradiation, etc.) and may not be exactly determined. Therefore, the $L1_0$ phase, either slightly stable or slightly metastable, is highly relevant to be considered in the low-temperature Fe-Ni phase diagram.

For the DFT predicted phase diagram, the major change due to the inclusion of the $L1_0$ phase is the absence of the $\alpha + L1_2$ two-phase region. This is because the predicted $T_c^{L1_0-\gamma}$ of 640 K is higher than the predicted eutectoid reaction temperature of 610 K. The disappearance of the $\alpha + L1_2$ equilibrium is expected because $L1_0$ -FeNi is increasingly more stable than $L1_2$ -FeNi₃ with increasing temperatures due to the larger vibrational entropy of mixing of the former (Fig. 5). Compared with Fig. 8, the predicted phase boundary $\alpha + L1_2/L1_2$ shifts closer to the experimental data of Ref. [67], while the phase boundary $\alpha/\alpha + L1_2$ is nearly unchanged.

The CALPHAD assessment predicts $L1_0$ decomposes into α and $L1_2$, but the decomposition occurs at a temperature less than half of the experimental $T_c^{L1_0-\gamma}$. Furthermore, $T_c^{L1_0-\gamma}$ determined from the CALPHAD phase diagram with only fcc phases is 311 K [15], still much lower than the measured $T_c^{L1_0-\gamma}$ of 593 K. The low $T_c^{L1_0-\gamma}$ from the CALPHAD prediction is due to the estimation of a lower 0 K mixing enthalpy for fcc disordered phases (Fig. 1).

As noted in Ref. [64], there is also another inconsistency in the CALPHAD assessment by Cacciamani *et al.* [15] at low temperatures. In Fig. 10, we show the experimental martensite start temperature M_S at which martensite starts to form, and theoretical T_0 , the temperature at which bcc and fcc phases with the same composition have the same ΔG_{mix} . For a given composition, the martensitic transformation starts below T_0 so that ΔG_{mix}^{fcc} is lower than ΔG_{mix}^{bcc} to provide a driving force to initiate nucleation. Therefore, the M_S curve should be always below the predicted T_0 curve. However, this is clearly not the case for the CALPHAD assessment, while the T_0 curve by DFT, though seems to be too “stiff,” is compatible with the M_S curve.

TABLE I. Experimental and theoretical $T_c^{L1_0-\gamma}$ and $T_c^{L1_2-\gamma}$. The results calculated with and without vibrational effects are shown.

Method	Expt.	CVM [17]		EAM [18]		DFT [20]		DFT (this work)	
		With S_{vib}	No S_{vib}	With S_{vib}	No S_{vib}	With S_{vib}	No S_{vib}	With S_{vib}	No S_{vib}
$T_c^{L1_2-\gamma}$	790 [5]	–	–	990	1660	–	–	830	1030
$T_c^{L1_0-\gamma}$	593 [8]	483	523	960	1800	560	1040	640	920

These results show that low-temperature thermodynamic properties predicted by the present DFT study are in better agreement with existing experimental data than the CALPHAD model by Cacciamani *et al.* [15]. Therefore, our DFT results can provide accurate data of disordered structures for a further optimization of CALPHAD parameters to improve its prediction at low and intermediate temperatures.

D. Role of the vibrational entropy on the order-disorder transition temperatures

The vibrational effects on the order-disorder transitions have been investigated in some theoretical studies. These results are compared with our results and experimental values in Table I.

All these studies agree that the inclusion of S_{vib} decreases $T_c^{L1_0-\gamma}$ and $T_c^{L1_2-\gamma}$ but disagree on the extent of the decrease. In the CVM study [17], $T_c^{L1_0-\gamma}$ is already lower than the experimental value and is further reduced by 40 K after introducing vibrational effects. It is noted that phase equilibrium calculated by CVM may not be in the equilibrium state as no local deformation was allowed in their calculations [17]. The EAM potential study [18] stresses the importance of vibrational entropy, but the estimated $T_c^{L1_0-\gamma}$ with and without vibrational contributions are too high compared with the experimental data, so these results may only be taken qualitatively. It is noted that the EAM study agrees with our calculations that the reduction in $T_c^{L1_0-\gamma}$ is larger than in $T_c^{L1_2-\gamma}$ with the inclusion of vibrational effects. In a recent DFT study on the $L1_0$ -disorder transition [20], the free energy, including the configurational, vibrational, electronic, and magnetic contributions, is calculated as a function of long-range order. According to this study, the configurational and vibrational effects are the most important and vibrational effects lower $T_c^{L1_0-\gamma}$ by 480 K compared to the value obtained including merely the configurational contribution. Our calculations also suggest that lattice vibrations reduce significantly the transition temperatures, with the amount of the decrease in $T_c^{L1_0-\gamma}$ lying between the results of Refs. [17,20].

The above theoretical results point out a significant role of S_{vib} on the prediction of order-disorder transition temperatures, though there is no quantitative agreement as the obtained values may be highly dependent of the approximation chosen. Consequently, it is worth recalling the approximations and possible sources of errors in the present study. Indeed, ΔH_{mix} is assumed to be constant, while its variation may be non-negligible near the phase transition temperatures according to the CALPHAD prediction by Cacciamani *et al.* [15]. The configurational entropy is calculated only at the low- (ordered structures) and high- (disordered structures)

temperature limits, while the true configurational entropy varies continuously between the two limits as the temperature changes. In addition, vibrational entropy is calculated within the harmonic approximation under constant volume and with perfectly FM order. Furthermore, electronic and magnetic entropies are neglected in this study. Based on these simple assumptions, our predicted phase diagrams below T_{Curie} and our order-disorder transition temperatures are in reasonable agreement with available experimental data, suggesting that the principal sources of entropy are captured, although some possible compensation of errors cannot be totally excluded. A reliable description of various contributions may require very accurate effective interaction models. On the experimental side, the measurements by Lucas *et al.* [54] do not allow us to draw definite conclusions on the vibrational effects because the experimental ordered sample was only partially ordered. Therefore, further experimental and theoretical efforts are needed to elucidate the effects of lattice vibrations.

V. CONCLUSION

Disordered bcc and fcc Fe-Ni structures (SQSs) with various magnetic states are studied by means of DFT calculations for the whole concentration range. The obtained results together with the properties of the ordered phases provide a comprehensive understanding of the phase stability of Fe-Ni alloys below the Curie temperatures.

Ground-state properties are calculated for the bcc FM and fcc AFD SQSs with up to 50% Ni and the fcc FM SQSs over the whole concentration range. The results of the mixing enthalpy provide a complete picture for the ground-state energetic landscape, i.e., the relative energy between various phases (bcc vs. fcc, ordered vs. disordered, antiferromagnetic vs. ferromagnetic states). Comparisons of the obtained mixing enthalpies of fcc structures with those from previous semiempirical studies show a qualitative agreement but with considerable quantitative differences in the concentrated region, which can impact on the finite-temperature phase stability.

The systematic comparison of the magnetization of the predicted magnetic ground state of bcc and fcc disordered phases with the experimental data exhibits an excellent agreement, confirming the representability of the assumed SQSs for solid solutions for the finite-temperature phase stability studies. Some locally antiferromagnetic fcc structures are proposed to approach experimental magnetization in the Invar region, while their energetic stability is strongly sensitive to the exchange-correlation functional adopted within DFT.

We confirm that $L1_0$ -FeNi and $L1_2$ -FeNi₃ are the only ground states of Fe-Ni alloys. The vibrational entropies of these ordered phases and several bcc and fcc FM disordered structures are evaluated as functions of temperatures within

the harmonic approximation. The comparison with the experimental entropies at 300 K shows an overall good agreement. The vibrational entropy of mixing of all the structures is always positive and saturates above 300 K, being larger in the SQSs than in the ordered structures. Due to a relatively large difference of vibrational entropies between the ordered and disordered structures, the vibrational entropy, often neglected in previous studies, is found to reduce the predicted order-disorder transition temperatures $T_c^{L1_2-\gamma}$ and $T_c^{L1_0-\gamma}$ by 200 and 280 K, respectively. The present study thus indicates a strong effect of vibrational entropy on the order-disorder transitions.

Free energies of mixing of bcc and fcc FM disordered structures are estimated by combining the calculated ground-state mixing enthalpy and the entropy of mixing, which is approximated as the sum of the vibrational entropy of mixing and ideal configurational entropy. From them, the theoretical Fe-Ni phase diagrams below the Curie temperatures are constructed and agree well with the experimental phase boundaries below 700 K and the measured order-disorder transition temperatures. Such an agreement suggests that the main contributions to the free energy have been captured. The effects of magnetic disorder on phase stability are also discussed in the light of the theoretical-experimental differences. In particular,

it is shown that magnetic disorder can have a major impact on the solubility of Ni in bcc Fe-Ni alloys.

Compared with a recent CALPHAD prediction, our results agree better with the experimental data such as the minimum solubility of Ni in $L1_2$, the phase boundaries of $L1_2 + \gamma_{FM}$ two-phase region, and the $L1_0$ -disorder transition temperature. These deviations by CALPHAD may be due to the inaccurate description of disordered structures. Therefore, the present results point out the necessity of including accurate data of Fe-Ni random solid solutions, in addition to information on ordered phases, as input data for CALPHAD and other semiempirical thermodynamic models.

ACKNOWLEDGMENTS

This work was performed using DARI-GENCI sources under the A0050906020 project, and the CINECA-MARCONI supercomputer within the SISTEEL project. The research leading to these results has been partially carried out in the frame of EERA Joint Program for Nuclear Materials and is partly funded by the European Commission HORIZON 2020 Framework Programme under Grant Agreement No. 755269. We thank our colleagues Frdric Soisson and Yimi Wang for the fruitful discussions.

-
- [1] C. É. Guillaume, C.R. Acad. Sci. **125**, 18 (1897).
 [2] E. Wassermann, *J. Magn. Magn. Mater.* **100**, 346 (1991).
 [3] H. Arnold and G. Elmen, *J. Franklin Inst.* **195**, 621 (1923).
 [4] L. J. Swartzendruber, V. P. Itkin, and C. B. Alcock, *J. Phase Equilib.* **12**, 288 (1991).
 [5] J. Van deen and F. Van Der Woude, *Acta Metall.* **29**, 1255 (1981).
 [6] K. B. Reuter, D. B. Williams, and J. I. Goldstein, *Metall. Trans. A* **20**, 719 (1989).
 [7] C. W. Yang, D. B. Williams, and J. I. Goldstein, *J. Phase Equilib.* **17**, 522 (1996).
 [8] J. Paulevé, D. Dautreppe, J. Laugier, and L. Néel, *J. Phys. Rad.* **23**, 841 (1962).
 [9] P. Munroe and M. Hatherly, *Scr. Metall. Mater.* **32**, 93 (1995).
 [10] R. A. Jago and P. L. Rossiter, *Phys. Status Solidi* **73**, 497 (1982).
 [11] L. T. Belkacemi, E. Meslin, B. Décamps, B. Radiguet, and J. Henry, *Acta Mater.* **161**, 61 (2018).
 [12] Y. Mishin, M. J. Mehl, and D. A. Papaconstantopoulos, *Acta Mater.* **53**, 4029 (2005).
 [13] S. V. Barabash, R. V. Chepulskii, V. Blum, and A. Zunger, *Phys. Rev. B* **80**, 220201(R) (2009).
 [14] J. S. Wróbel, D. Nguyen-Manh, M. Y. Lavrentiev, M. Muzyk, and S. L. Dudarev, *Phys. Rev. B* **91**, 024108 (2015).
 [15] G. Cacciamani, A. Dinsdale, M. Palumbo, and A. Pasturel, *Intermetallics* **18**, 1148 (2010).
 [16] T. Mohri and Y. Chen, *J. Alloys Compd.* **383**, 23 (2004).
 [17] T. Mohri, Y. Chen, and Y. Jufuku, *Calphad* **33**, 244 (2009).
 [18] G. Bonny, R. C. Pasianot, and L. Malerba, *Model. Simul. Mater. Sci. Eng.* **17**, 025010 (2009).
 [19] M. Y. Lavrentiev, J. S. Wróbel, D. Nguyen-Manh, and S. L. Dudarev, *Phys. Chem. Chem. Phys.* **16**, 16049 (2014).
 [20] L.-Y. Tian, H. Levämäki, O. Eriksson, K. Kokko, Á. Nagy, E. K. Délczeg-Czirják, and L. Vitos, *Sci. Rep.* **9**, 8172 (2019).
 [21] A. Zunger, S.-H. Wei, L. G. Ferreira, and J. E. Bernard, *Phys. Rev. Lett.* **65**, 353 (1990).
 [22] P. E. Blöchl, *Phys. Rev. B* **50**, 17953 (1994).
 [23] G. Kresse and D. Joubert, *Phys. Rev. B* **59**, 1758 (1999).
 [24] G. Kresse and J. Hafner, *Phys. Rev. B* **47**, 558 (1993).
 [25] G. Kresse and J. Furthmüller, *Comput. Mater. Sci.* **6**, 15 (1996).
 [26] G. Kresse and J. Furthmüller, *Phys. Rev. B* **54**, 11169 (1996).
 [27] J. P. Perdew, K. Burke, and M. Ernzerhof, *Phys. Rev. Lett.* **77**, 3865 (1996).
 [28] M. Methfessel and A. T. Paxton, *Phys. Rev. B* **40**, 3616 (1989).
 [29] H. J. Monkhorst and J. D. Pack, *Phys. Rev. B* **13**, 5188 (1976).
 [30] J. M. Cowley, *Phys. Rev.* **77**, 669 (1950).
 [31] E. Martinez, C. C. Fu, M. Levesque, M. Nastar, and F. Soisson, *Solid State Phenom.* **172–174**, 1016 (2011).
 [32] A. Togo and I. Tanaka, *Scr. Mater.* **108**, 1 (2015).
 [33] See Supplemental Material at <http://link.aps.org/supplemental/10.1103/PhysRevMaterials.4.023606> for the data on the ground-state properties of pure, ordered and disordered phases, the discussion about LAF structures and the use of off-stoichiometric structures.
 [34] Q. Chen and B. Sundman, *J. Phase Equilib.* **22**, 631 (2001).
 [35] Y. Tsunoda, *J. Phys.: Condens. Matter* **1**, 10427 (1989).
 [36] D. Qian, X. F. Jin, J. Barthel, M. Klaua, and J. Kirschner, *Phys. Rev. Lett.* **87**, 227204 (2001).
 [37] C. S. Tian, D. Qian, D. Wu, R. H. He, Y. Z. Wu, W. X. Tang, L. F. Yin, Y. S. Shi, G. S. Dong, X. F. Jin, X. M. Jiang, F. Q. Liu, H. J. Qian, K. Sun, L. M. Wang, G. Rossi, Z. Q. Qiu, and J. Shi, *Phys. Rev. Lett.* **94**, 137210 (2005).
 [38] D. Rancourt, S. Chehab, and G. Lamarche, *J. Magn. Magn. Mater.* **78**, 129 (1989).

- [39] T. P. C. Klaver, D. J. Hepburn, and G. J. Ackland, *Phys. Rev. B* **85**, 174111 (2012).
- [40] I. A. Abrikosov, A. E. Kissavos, F. Liot, B. Alling, S. I. Simak, O. Peil, and A. V. Ruban, *Phys. Rev. B* **76**, 014434 (2007).
- [41] J. Crangle and G. C. Hallam, *Proc. R. Soc. Lond. A* **272**, 119 (1963).
- [42] H. Asano, *J. Phys. Soc. Jpn.* **27**, 542 (1969).
- [43] E. Owen and A. Sully, *Philos. Mag. J. Sci.* **31**, 314 (1941).
- [44] V.-T. Tran, C.-C. Fu, and K. Li, *Comput. Mater. Sci.* **172**, 109344 (2020).
- [45] Y. Wang, G. M. Stocks, D. M. C. Nicholson, W. A. Shelton, V. P. Antropov, and B. N. Harmon, *J. Appl. Phys.* **81**, 3873 (1997).
- [46] A. V. Ruban, S. Khmelevskiy, P. Mohn, and B. Johansson, *Phys. Rev. B* **76**, 014420 (2007).
- [47] M. Van Schilfgaarde, I. A. Abrikosov, and B. Johansson, *Nature* **400**, 46 (1999).
- [48] C. S. Wang, B. M. Klein, and H. Krakauer, *Phys. Rev. Lett.* **54**, 1852 (1985).
- [49] E. L. P. Blancá, C. O. Rodríguez, J. Shitu, and D. L. Novikov, *J. Phys.: Condens. Matter* **13**, 9463 (2001).
- [50] F. Körmann, A. Dick, B. Grabowski, B. Hallstedt, T. Hickel, and J. Neugebauer, *Phys. Rev. B* **78**, 033102 (2008).
- [51] F. Körmann, A. Dick, B. Grabowski, T. Hickel, and J. Neugebauer, *Phys. Rev. B* **85**, 125104 (2012).
- [52] F. Körmann, B. Grabowski, B. Dutta, T. Hickel, L. Mauger, B. Fultz, and J. Neugebauer, *Phys. Rev. Lett.* **113**, 165503 (2014).
- [53] F. Körmann, P.-W. Ma, S. L. Dudarev, and J. Neugebauer, *J. Phys.: Condens. Matter* **28**, 076002 (2016).
- [54] M. S. Lucas, L. Mauger, J. A. Muñoz, I. Halevy, J. Horwath, S. L. Semiatin, S. O. Leontsev, M. B. Stone, D. L. Abernathy, Y. Xiao, P. Chow, and B. Fultz, *J. Appl. Phys.* **113**, 17A308 (2013).
- [55] D. A. Porter, K. E. Easterling, and K. E. Easterling, *Phase Transformations in Metals and Alloys (Revised Reprint)*, 3rd ed. (CRC Press, Boca Raton, 2009), pp. 1–521.
- [56] J. A. Muñoz, M. S. Lucas, O. Delaire, M. L. Winterrose, L. Mauger, C. W. Li, A. O. Sheets, M. B. Stone, D. L. Abernathy, Y. Xiao, P. Chow, and B. Fultz, *Phys. Rev. Lett.* **107**, 115501 (2011).
- [57] S. Lintzen, J. von Appen, B. Hallstedt, and R. Dronskowski, *J. Alloys Compd.* **577**, 370 (2013).
- [58] J. B. Piochaud, T. P. C. Klaver, G. Adjanor, P. Olsson, C. Domain, and C. S. Becquart, *Phys. Rev. B* **89**, 024101 (2014).
- [59] S. Zhao, G. M. Stocks, and Y. Zhang, *Phys. Chem. Chem. Phys.* **18**, 24043 (2016).
- [60] S. Chentouf and P. Maugis, *Comput. Mater. Sci.* **126**, 82 (2017).
- [61] A. Schneider, C.-C. Fu, and C. Barreateau, *Phys. Rev. B* **98**, 094426 (2018).
- [62] S. Mahmoud and N. Mousseau, *Materialia* **4**, 575 (2018).
- [63] S. Zhao, Y. Osetsky, and Y. Zhang, *J. Alloys Compd.* **805**, 1175 (2019).
- [64] W. Xiong, H. Zhang, L. Vitos, and M. Selleby, *Acta Mater.* **59**, 521 (2011).
- [65] T. Mohri, *J. Mater. Sci.* **50**, 7705 (2015).
- [66] A. D. Romig and J. I. Goldstein, *Metall. Trans. A* **11**, 1151 (1980).
- [67] T. Heumann and G. Karsten, *Arch. für das Eisenhüttenwes.* **34**, 781 (1963).
- [68] I. Ohnuma, S. Shimenouchi, T. Omori, K. Ishida, and R. Kainuma, *Calphad* **67**, 101677 (2019).
- [69] J. Zhang, D. B. Williams, and J. I. Goldstein, *Metall. Mater. Trans. A* **25**, 1627 (1994).
- [70] W. Xiong, M. Selleby, Q. Chen, J. Odqvist, and Y. Du, *Crit. Rev. Solid State Mater. Sci.* **35**, 125 (2010).
- [71] G. Cacciamani, J. De Keyzer, R. Ferro, U. Klotz, J. Lacaze, and P. Wollants, *Intermetallics* **14**, 1312 (2006).
- [72] O. K. von Goldbeck and O. K. von Goldbeck, *IRON–Binary Phase Diagrams* (Springer, Berlin, 1982), pp. 73–78.
- [73] I. V. Vernyhora, D. Ledue, R. Patte, and H. Zapolsky, *J. Magn. Mater.* **322**, 2465 (2010).
- [74] R. J. Wakelin and E. L. Yates, *Proc. Phys. Soc. Sect. B* **66**, 221 (1953).
- [75] M. Peschard, *Rev. Mét. Paris* **22**, 490 (1925).
- [76] J. Petersen, M. Aydin, and J. Knudsen, *Phys. Lett. A* **62**, 192 (1977).
- [77] R. S. Clarke and E. R. D. Scott, *Am. Mineral.* **65**, 624 (1980).
- [78] R. B. Scorzelli, *Hyperfine Interact.* **110**, 143 (1997).
- [79] A. Makino, P. Sharma, K. Sato, A. Takeuchi, Y. Zhang, and K. Takenaka, *Sci. Rep.* **5**, 16627 (2015).
- [80] S. Lee, K. Edalati, H. Iwaoka, Z. Horita, T. Ohtsuki, T. Ohkochi, M. Kotsugi, T. Kojima, M. Mizuguchi, and K. Takanashi, *Philos. Mag. Lett.* **94**, 639 (2014).
- [81] K. B. Reuter, D. B. Williams, and J. I. Goldstein, *Metall. Trans. A* **20**, 711 (1989).
- [82] A. Chamberod, J. Laugier, and J. M. Penisson, *J. Magn. Mater.* **10**, 139 (1979).
- [83] T. Horiuchi, M. Igarashi, F. Abe, and T. Mohri, *Calphad* **26**, 591 (2002).
- [84] I. Ohnuma, R. Kainuma, and K. Ishida, in *CALPHAD and Alloy Thermodynamics as held at the 2002 TMS Annual Meeting* (2002), pp. 61–78.